Evaluation of regional cloud feedbacks using single-column models

Anthony D. Del Genio
NASA Goddard Institute for Space Studies, New York, New York, USA

Audrey B. Wolf and Mao-Sung Yao
SGT Inc., Institute for Space Studies, New York, New York, USA

Received 13 May 2004; revised 10 September 2004; accepted 21 September 2004; published 31 March 2005.

[1] Cloud feedbacks in a warmer climate have not yet been constrained by models or observations. We present an approach that combines a general circulation model (GCM), single-column model (SCM), satellite and surface remote sensing data, and analysis product to infer regional cloud feedbacks and evaluate model simulations of them. The Atmospheric Radiation Measurement (ARM) Program Southern Great Plains (SGP) continuous forcing product, derived from a mesoscale analysis constrained by top-of-atmosphere and surface data, provides long-term advective forcing that links the models to the data. We drive an SCM with the continuous forcing for 10 cold season months in which synoptic forcing dominates the meteorology. Cloud feedbacks in midlatitude winter are primarily responses to changes in dynamical forcing. Thus we select times when observed advective forcing anomalies resemble doubled CO_2 advective forcing changes in the parent GCM. For these times we construct cloud type anomaly histograms in the International Satellite Cloud Climatology Project and Active Remotely Sensed Cloud Locations data sets and simulated versions of these histograms in the SCM. Comparison of the SCM subset to GCM doubled CO_2 cloud type changes tells us how relevant the selected times are to the GCM's cloud feedbacks, while comparisons of the SCM to the data tell us how well the model performs in these situations. The data suggest that in midlatitude winter, high thick clouds should increase while cirrus and low clouds decrease in upwelling regimes in a climate warming. Downwelling regime cloud feedbacks are dominated by changes in low clouds but are not as well constrained by the data.

Citation: Del Genio, A. D., A. B. Wolf, and M.-S. Yao (2005), Evaluation of regional cloud feedbacks using single-column models, *J. Geophys. Res.*, *110*, D15S13, doi:10.1029/2004JD005011.

1. Introduction

[2] Cloud parameterization advances in general circulation models (GCMs) over the past few decades have not been successful in narrowing uncertainties in predictions of cloud feedback in a changing climate. Single-column model (SCM) versions of GCMs and cloud-resolving models (CRMs) that crudely resolve cloud-scale dynamics have been used to simulate limited time periods, driven by field experiment data or enhanced soundings during Intensive Observation Periods (IOPs). These exercises have proven difficult to interpret, because model-data discrepancies can be due to inaccurate large-scale advective forcing, inaccurate model physics, or problems with the cloud data, and instantaneous model errors may not be climatically representative or diagnostic of problems with the model's cloud feedback. An approach that utilizes the strengths of complementary model and data types together might facilitate progress.

[3] There are no perfect proxies for an enhanced greenhouse gas climate in records of observed current climate variability. Climate change may manifest itself as a change in the frequency of occurrence of current atmospheric states, or as the onset of previously unrealized states [cf. *Bony et al.*, 2004]. It might be possible to learn something about cloud responses to external climate forcing if examples of internal forcing whose structure resembles that of the future climate can be identified in current climate records. In climate GCMs the direct radiative heating/cooling perturbation due to the greenhouse gas increase itself is small except near the surface. Instead, strong positive feedbacks associated with changes in water vapor and snow-sea ice are primarily responsible for the altered thermodynamic structure of the warmer climate. In many situations clouds are a tracer of the general circulation, i.e., they are a response to the advection of heat and moisture. Cloud feedbacks can therefore be viewed as the response to anomalous advective tendencies caused by climate changes in the circulation and the temperature and moisture gradients along which they advect. If we define those anomalous advective tendencies in GCM climate change simulations and can find current climate examples of similar tendencies, it should be possible to use simultaneous cloud observations to define the cloud type changes that are consistent with the altered dynamical state.

[4] A major drawback to such an approach is the general unavailability of accurate instantaneous information about

Copyright 2005 by the American Geophysical Union.
0148-0227/05/2004JD005011

the general circulation in most climate regimes. Reanalysis products are most tightly constrained by observations in northern midlatitudes, and even there, the dynamical response is often muted in the presence of unresolved diabatic heating. IOPs with a large-scale array of enhanced soundings provide more accurate dynamical tendencies but also not without errors and with at best only an example or two of the desired dynamical conditions given their short duration. A recent promising alternative is the "continuous forcing" data set derived by *Xie et al.* [2004] at the Atmospheric Radiation Measurement (ARM) Program's Southern Great Plains (SGP) site. The continuous forcing product modifies the mesoscale analysis from the Rapid Update Cycle 2 (RUC-2) system using surface and top-of-atmosphere data and a variational analysis approach to balance observed column budgets of mass, heat, moisture and momentum. Xie et al. show that the continuous forcing product is often of comparable quality to that from IOPs, but with the advantage of being available for climatically significant periods of time (two years have been processed thus far).

[5] This paper describes a first attempt to implement the philosophy described above to observationally constrain regional cloud feedbacks and to evaluate the ability of the Goddard Institute for Space Studies (GISS) SCM to simulate them. Section 2 describes the models and data sets and the analysis approach in detail. Section 3 documents the observed and model-simulated mean dynamical and cloud states. Section 4 presents observed and simulated cloud type anomalies for time periods representative of forced climate change. Section 5 explores the sensitivity of the model results to vertical resolution and advective forcing. Section 6 discusses sensitivity tests exploring differences between two cloud data sets and between the data and the SCM. Section 7 discusses the implications of our work for cloud parameterization development and climate sensitivity assessment.

2. Approach

[6] Weather at the SGP site is controlled by baroclinic wave activity and frontal passages. Superimposed diurnal variations and deep convection occur more frequently in summer, while winter variability is more purely synoptic in nature. It is during winter that we expect clouds to be most nearly a response to synoptic forcing rather than a determinant of the forcing. Thus we test our approach by selecting 5 cold season months of continuous forcing (January–March and November–December) in the two available years (1999–2000) to drive the GISS SCM for a total of 10 simulated months. The SCM physics is similar to that in the SI2000 version of the GISS GCM, but includes updated cloud and convection physics, based on that described by *Del Genio et al.* [2005]. The SCM has performed well in ARM intercomparisons [cf. *Xie et al.*, 2002]. We run the SCM with 35 layers matched to the resolution of the hourly continuous forcing advective tendencies of temperature and specific humidity. The SCM is re-initialized every 24 hours with the observed thermodynamic profiles to avoid obscuration of the cloud response by climate drift on long timescales.

[7] We use two complementary data sets to characterize the cloud structure at the SGP. The International Satellite Cloud Climatology Project (ISCCP) D1 data [*Rossow and Schiffer*, 1999] provide joint distributions of cloud top pressure and total column optical thickness at ~5 km resolution sampled to ~30 km every 3 hours during daytime for areas comparable to the size of a GCM grid box. The top pressure corresponds to the highest cloud; multilayer cloud situations cannot be identified. The retrieval, using visible and window infrared radiances, does not detect very optically thin clouds and sometimes incorrectly locates the top of clouds it detects, due to inadequate information about humidity and temperature structure or multiple cloud layers.

[8] The Active Remotely Sensed Cloud Layers (ARSCL) product [*Clothiaux et al.*, 2000] combines millimeter cloud radar, micropulse lidar, and laser ceilometer data to derive a best estimate of the altitudes of all cloud bases and tops in a narrow field of view looking upward at the SGP Central Facility. The results are considered accurate except for occasional underestimates of cloud top in deep heavily precipitating cloud systems and for thin, low radar reflectivity clouds above thick lower clouds. However, they are representative of an area much smaller than a GCM grid box. Comparison to the SCM is simplified by accumulating statistics over many events rather than making instantaneous comparisons. ARSCL cloud profiles are compiled at 10-s intervals; we aggregate them over each hour and create joint distributions of cloud top height and total cloud physical thickness (the sum of all individual layer thicknesses) as a geometric cloud property counterpart to the ISCCP radiative property distributions. We only use ARSCL data at times when the cloud radar determines the cloud top; over our hourly aggregating time interval radar-determined cloud tops are almost always available.

[9] To compare the satellite observations to the model, hourly SCM cloud fields are diagnosed using the ISCCP simulator [*Klein and Jakob*, 1999; *Webb et al.*, 2001]. We also take 100 subgrid columns of overlapping cloud produced by the ISCCP simulator as input to create a crude "ARSCL simulator." For each hour we randomly select one column plus the 3 adjacent columns as a representative sample of the atmospheric volume observed by the active sensors over the hour, given typical cold season midtropospheric wind speeds at the SGP. No attempt is made to simulate incorrect ARSCL retrievals of cloud top under the conditions described earlier.

[10] From this 10-month record of cold season cloudiness variability, we select time periods that are most relevant for understanding cloud feedbacks in a climate change. To do so, we use equilibrium $2 \times CO_2$ and $1 \times CO_2$ simulations of the GISS GCM. Each equilibrated run is sampled hourly for 10 years at the SGP and three nearby grid boxes. At each grid box and time step advective tendencies of temperature and humidity and ISCCP/ARSCL simulator cloud histograms are saved. The differences between these quantities for the warmer minus control climate, averaged over the ten years, define the climate change advective forcing anomalies and the associated cloud response that determines the regional cloud feedback. We separate the anomalies by the sign of the 500 mb vertical velocity ω, since upwelling and downwelling segments of baroclinic waves have characteristically different cloud structures and might not respond in the same way to climate forcing. The anomalies are interpolated to the vertical resolution of the continuous forcing.

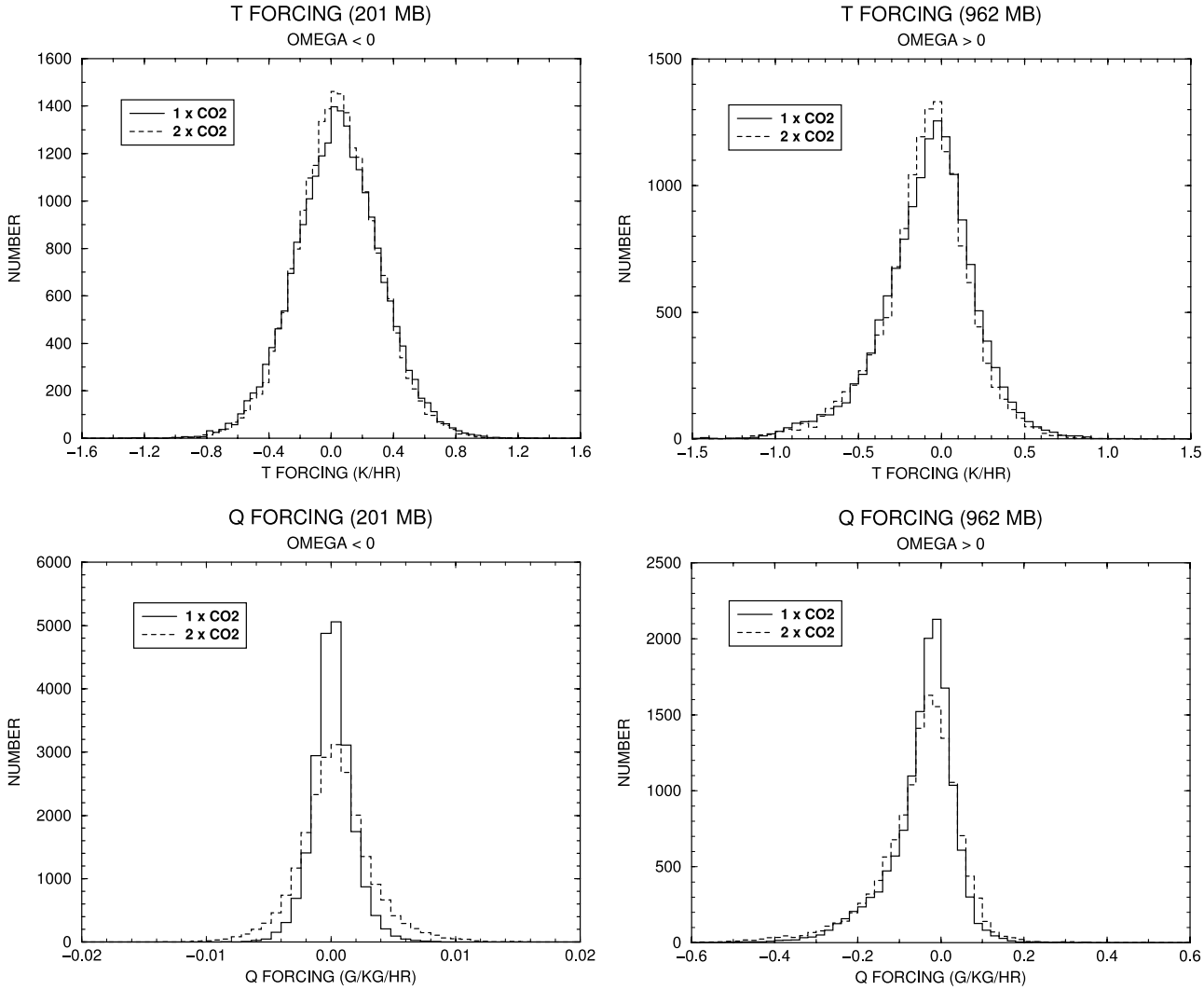

Figure 1. Histograms of (upper panels) advective temperature and (lower panels) advective moisture forcing at 201 mb for $\omega < 0$ (left panels) and at 962 mb for $\omega > 0$ (right panels) for the GCM $1 \times CO_2$ (solid) and $2 \times CO_2$ (dashed) climates.

[11] We then correlate the vertical profiles of the time mean warm minus control advective tendency differences with the instantaneous advective tendency anomalies in the continuous forcing data (relative to the 10-month mean tendency profiles) for $\omega < 0$ and $\omega > 0$. Those time steps for which the vertical structure of temperature and moisture tendency anomaly profiles is correlated with those from the climate change simulation at the 95% confidence level or higher (correlation coefficient $r > 0.418$) are selected as being most representative of the vertical structure of the climate change in forcing. The observed ISCCP/ARSCL histograms averaged over those times are interpreted as an indicator of what the atmosphere's actual regional response to such climate forcings would look like. Comparison of these observed cloud anomalies to those simulated by the SCM at the same times tests the fidelity of the model cloud feedbacks. Finally, comparison of the SCM-simulated cloud anomalies to the $2 \times CO_2$ cloud changes tells us how relevant the observed current climate advective forcing anomalies are to the processes that determine the cloud feedbacks in the climate change simulation.

[12] Several caveats must be stated.

[13] 1. A GCM climate change simulation is only available for an earlier version of the model physics [cf. *Yao and Del Genio*, 2002] at slightly coarser horizontal resolution and much coarser vertical resolution than for the SCM and continuous forcing ($4° \times 5° \times 9L$ as opposed to $\sim 3° \times 3° \times 35L$). Several effects of the vertical resolution difference in particular will be apparent in what follows.

[14] 2. Climate change is actually a shift and/or shape change in the entire probability density function (pdf) of advective tendencies rather than just a change in the mean values for upwelling and downwelling situations (Figure 1). Ideally one would treat the changes separately for weak, intermediate and strong vertical velocities of both signs. However, the 2-year length of the currently available continuous forcing data set does not allow us to accumulate sufficient statistics in a large number of ω bins.

[15] 3. We have ignored the contributions of surface turbulent fluxes and the $2 \times CO_2$ radiative heating anomaly itself to the tendencies. In midlatitude winter, surface fluxes should either be small or correlated with specific dynamical

anomalies (e.g., cold air outbreaks), so the former should not be an issue. The radiative heating anomaly is an order of magnitude smaller than the peak dynamical heating anomaly, but it is nonnegligible relative to the advective anomaly near the surface.

[16] 4. The best matches to the climate change advective tendencies in the continuous forcing are not perfect, and this accounts for some of the differences we observe in the sections that follow.

[17] 5. Current climate variability is much stronger than forced climate changes, so any nonlinearity in cloud response will hinder comparisons to the GCM.

3. Mean Forcings and Cloud Distributions

[18] Figure 2 shows the 10-month mean continuous forcing temperature and moisture advective tendency profiles for $\omega < 0$ and $\omega > 0$. Temperature tendencies are characterized by adiabatic cooling, peaking near 500 mb, in upwelling regimes but changing sign to adiabatic warming near 300 mb, presumably a signature of sloping frontal surfaces. In downwelling regimes the opposite is true although the forcing has a broader and lower altitude peak and slightly smaller peak magnitudes. Moisture tendencies are defined by moistening/drying in upwelling/downwelling situations, respectively, again with weaker magnitude and a lower altitude peak in downwelling cases (900 versus 750 mb).

[19] Also shown for comparison in Figure 2 are the control simulation advective tendency profiles from the free-standing GCM for the SGP region. GCM advective forcings have the same general pattern as those in the continuous forcing but are noticeably weaker and shallower in upwelling regions. This may be a reflection of the inability of coarse-resolution climate GCMs to resolve mesoscale secondary circulations along fronts. In fact the problem may be more widespread; even the mesoscale RUC-2 analysis underestimates the forcing in upwelling situations when variational constraints are not applied [*Xie et al.*, 2004].

[20] Figure 3 shows mean observed and simulated cloud property histograms for the $\omega < 0$ regime. ISCCP retrievals (upper left) suggest 4 dominant cloud types in these situations: low to midlevel optically thick clouds (suggestive of stratus or stratocumulus) with tops near ~600–700 mb, high top optically thick clouds (nimbostratus and perhaps some cumulonimbus) with tops near ~300–400 mb, optically thin cirrus at similar top pressures, and a class of very optically thin clouds near the tropopause. The latter cloud category is known to include some artifacts associated with situations in which ISCCP cannot uniquely identify the actual cloud top.

[21] ARSCL retrievals (Figure 3) indicate some similarities and some differences in this overall picture, keeping in mind the different space and timescales associated with the passive and active sensors. ARSCL detects physically thin and thick high clouds with tops at ~9–11 km, consistent with but a bit higher than two of the ISCCP high cloud types. However ARSCL detects no tropopause thin cirrus. Such cirrus may be below the radar reflectivity detection threshold, or it may be that this feature is an artifact of ISCCP limitations in optically thin cloud situations. ARSCL

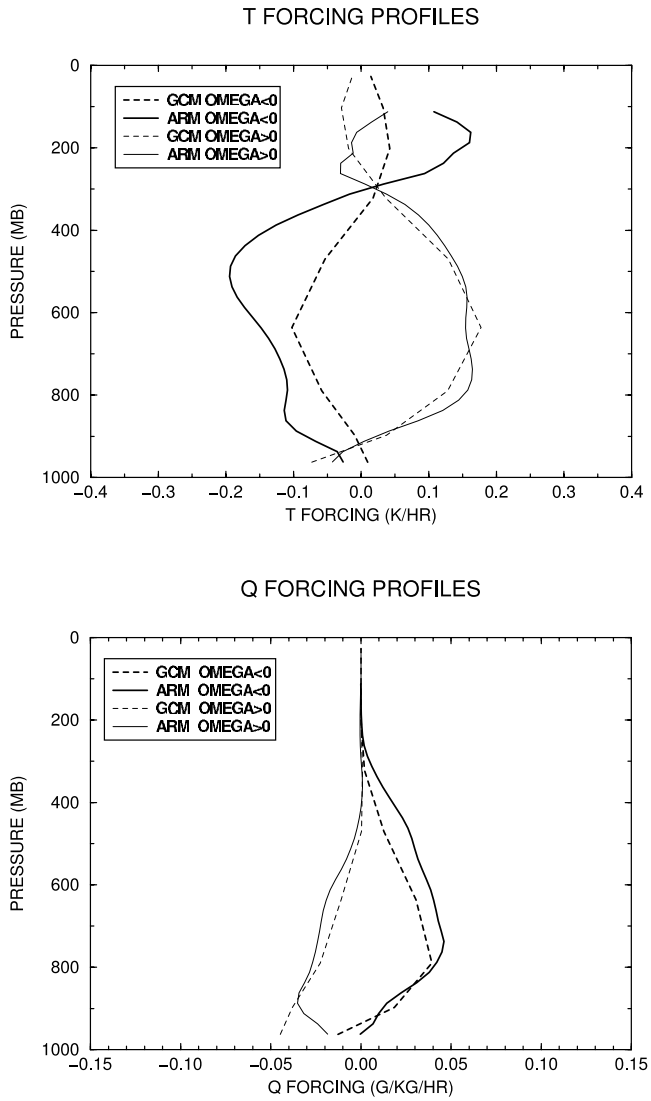

Figure 2. Cold season mean advective tendencies of (top) temperature and (bottom) specific humidity for the SGP region. Solid curves, ARM continuous forcing; dashed curves, GISS GCM climatology; bold curves, 500 mb $\omega < 0$; light curves, 500 mb $\omega > 0$.

detects a low physically thin cloud category but with tops at ~1–2 km, well below the ~600–700 mb ISCCP inference. The SCM (Figure 3) does a fairly good job in simulating the observed cloud types. It captures both high cloud types at the correct top pressures, though its optically thin clouds are too thin and its optically thick clouds too thick. It also simulates the low thin cloud category but at slightly lower altitude than inferred from the ARSCL data. The SCM does not simulate the occasional presence of midlevel, moderate thickness clouds that ARSCL detects.

[22] The GCM (Figure 3) differs from the SCM and the observations in its inability to make thin cirrus. This may be a consequence of its coarse resolution in two ways: the weaker and shallower storms (Figure 2) that create a dry bias in the winter upper troposphere, and the thick (2–3 km) upper troposphere layers that prevent the production of physically thin clouds (although the GISS cloud parameter-

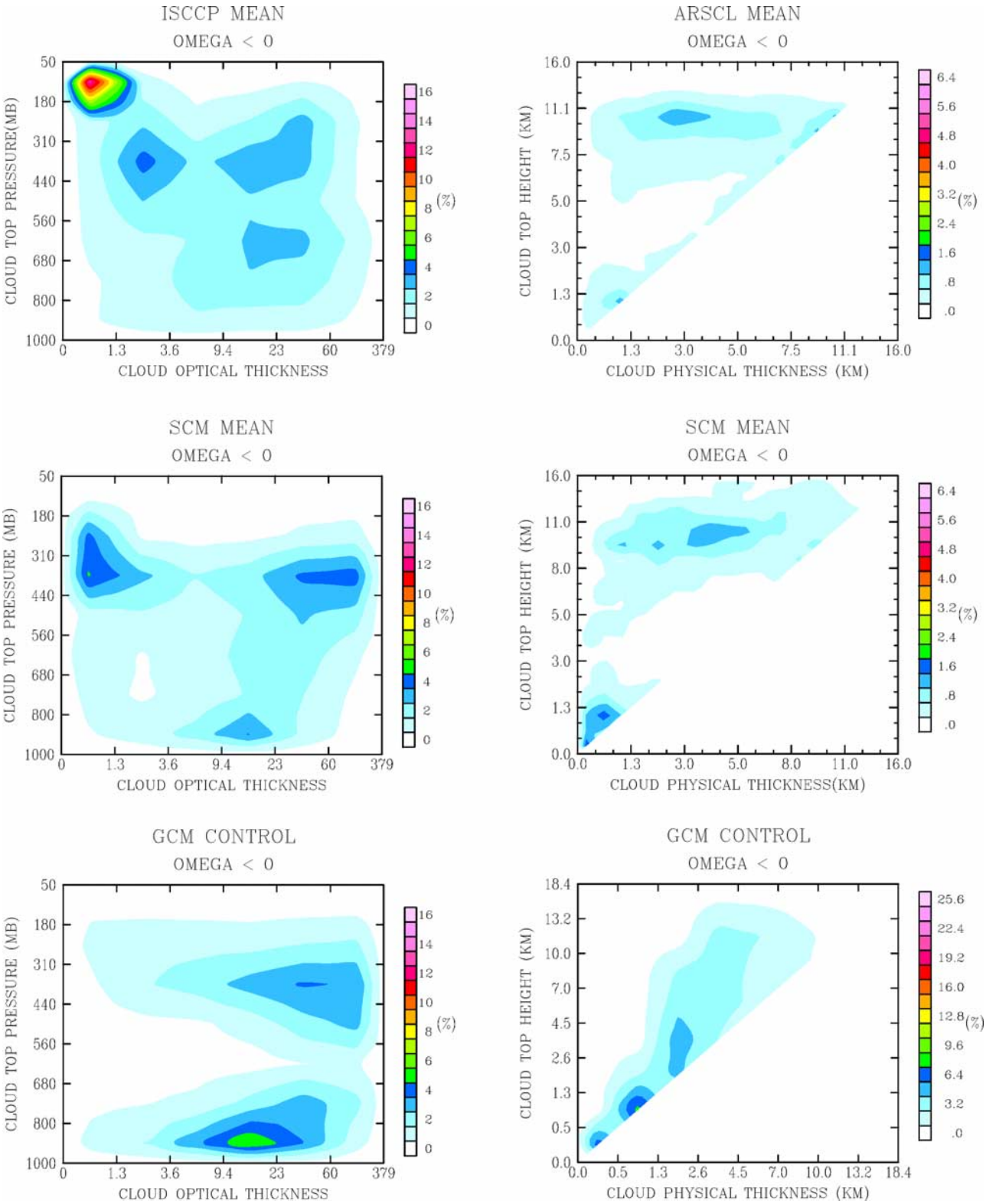

Figure 3. Cold season mean observed and simulated cloud property histograms for 500 mb $\omega < 0$. Top panels represent observations, middle panels the SCM simulation of the same time period, and bottom panels the GCM climatology. The left panels are ISCCP data and simulator results portrayed as frequency of occurrence (%) as a function of cloud top pressure (mb) and column optical thickness. The right panels are ARSCL data and simulator results portrayed as frequency of occurrence as a function of height of the highest cloud top (km) and total physical thickness of all cloudy layers (km). Note the different GCM ARSCL simulator color scale owing to the smaller number of GCM layers.

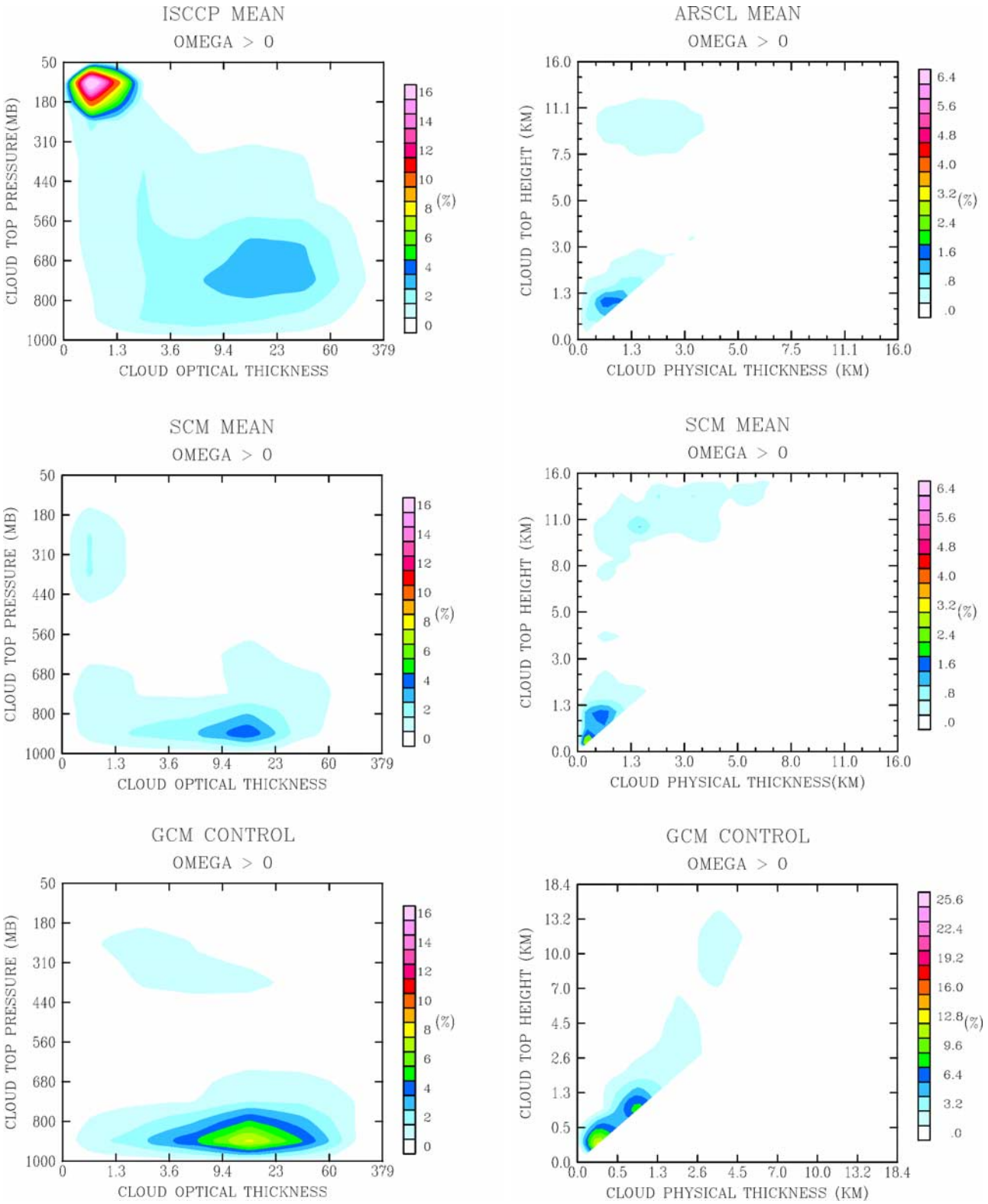

Figure 4. As in Figure 3 but for 500 mb $\omega > 0$.

ization tries to compensate by allowing for subgrid cloud thickness). The GCM's low clouds are also somewhat different from observed via the presence of a second peak near 0.5 km, another effect of its discretization.

[23] Figure 4 shows the same cloud distributions for the $\omega > 0$ regime. Not surprisingly, the major difference between this regime and the upwelling regime is the absence of high thick clouds and the less frequent occurrence of cirrus; the dominant cloud type is low physically thin but moderately optically thick stratus or stratocumulus. Many of the same ISCCP-ARSCL and SCM-GCM differences described earlier are seen in this regime as well. The

GCM overestimates low cloud in this regime, a behavior only slightly evident in the upwelling regime.

4. Forcing and Cloud Distribution Anomalies

[24] Figure 5 shows the advective tendency anomaly profiles defined by the 2 × CO_2 versus 1 × CO_2 GCM simulation differences for $\omega < 0$ and $\omega > 0$, as well as the average of all continuous forcing anomaly profiles that are highly correlated with the GCM climate change tendency anomalies. Two versions of the continuous forcing anomaly profiles are shown, one averaged over all highly correlated time steps (197 for $\omega < 0$, 263 for $\omega > 0$) and another for only those highly correlated time steps for which ISCCP histograms exist (29 for $\omega < 0$, 22 for $\omega > 0$). For ease of comparison the GCM climate change profiles in Figure 5 have been scaled by the ratio of the vertically integrated magnitudes of the continuous forcing anomalies to those for the much weaker climate change anomalies (23.98 and 13.68 for T forcing for $\omega < 0$ and $\omega > 0$, respectively, and 27.65 and 22.30 for q forcing for $\omega < 0$ and $\omega > 0$, respectively).

[25] GCM climate change advective anomalies in upwelling situations are characterized primarily by an upward shift in the level of peak adiabatic cooling and moistening. The lower troposphere signal consists of weak warming and cooling anomalies just above and below the 800 mb level, respectively, and moderate drying below the 800 mb level. The continuous forcing contains a number of instances of forcing anomalies whose middle and upper troposphere structure resembles that for the climate change, although the climate change anomalies are larger at higher levels. The best matches are less successful near the surface, consisting primarily of adiabatic warming and drying. The difference is partly compensated by the direct radiative warming due to doubling CO_2 which is felt mostly near the surface.

[26] In downwelling situations, the GCM climate change advective anomalies are just the opposite, defined by an upward shift in the adiabatic warming and drying peaks. The continuous forcing best matches are satisfactory for the q forcing profile but not as successful for the T forcing profile, the latter being shifted in the negative direction at all altitudes relative to the climate change profiles, i.e., weak upper level warming anomalies and stronger lower troposphere cooling anomalies.

[27] Figures 6 and 7 show the contributions to the forcing anomalies from horizontal and vertical advection, as well as the part of the vertical advection anomalies due to the vertical velocity anomaly, for the continuous forcing and the GCM. The continuous forcing anomalies (Figure 6) are instantaneous weather deviations from the mean state, so the total forcing anomalies can be large. For $\omega < 0$ vertical advection is more important, while for $\omega > 0$ horizontal advection dominates. In both cases the vertical advection anomaly depends mostly on the change in vertical velocity, with the change in temperature and moisture gradient playing a significant role only in the upper troposphere. By contrast, the GCM climate changes in advective forcing (Figure 7) are small differences between two equilibrium states, so the total forcing anomalies are much smaller, with horizontal and vertical advection anomalies nearly canceling for temperature and at least partly offsetting for humidity. The vertical velocity change is small and of opposite sign to the mean in each regime, so the advection changes in this case are controlled by the CO_2-driven changes in temperature and moisture gradients. Thus the continuous forcing anomalies are only proxies for climate change, not an attempt to find identical conditions in the current climate. The difference is largely irrelevant for our purposes because most cloud parameterizations respond

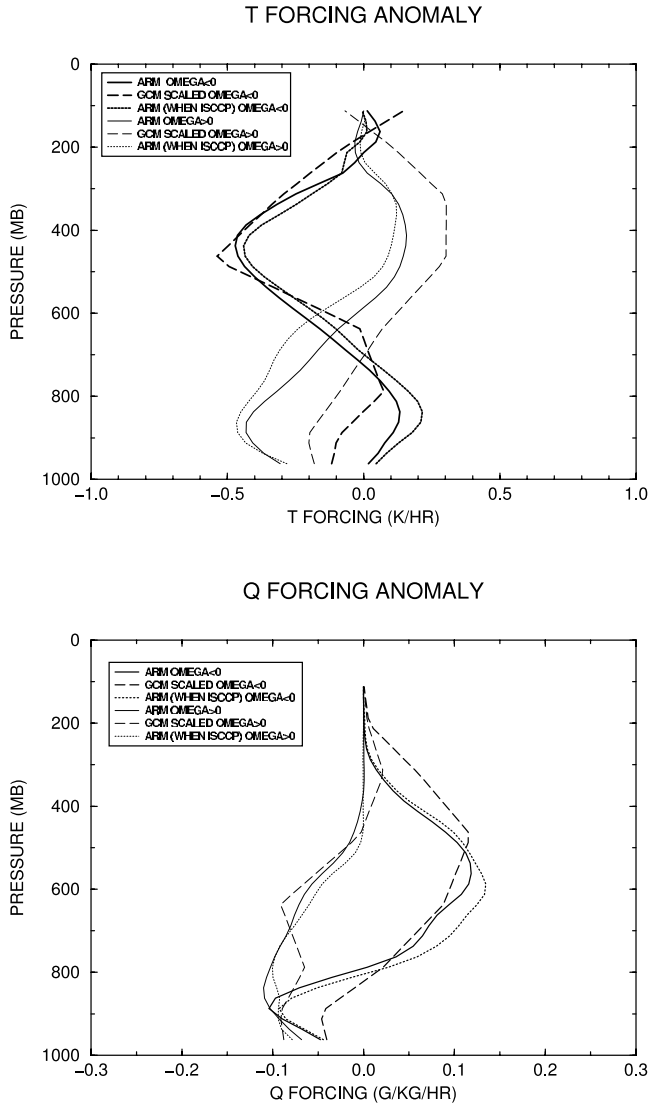

Figure 5. Anomalies of advective tendencies of (top) temperature and (bottom) specific humidity for the SGP region relative to the mean profiles in Figure 2 for times when the continuous forcing advective tendency anomalies are correlated at the 95% confidence level or greater with GCM 2 × CO_2 versus 1 × CO_2 advective tendency differences. Solid curves, ARM continuous forcing anomalies for all highly correlated times; dotted curves, ARM continuous forcing anomalies for highly correlated times that have ISCCP observations; dashed curves, GCM climate change differences; bold curves, 500 mb $\omega < 0$; light curves, 500 mb $\omega > 0$. The GCM curves have been scaled to have the same vertically integrated magnitude as the continuous forcing profiles for ease of comparison.

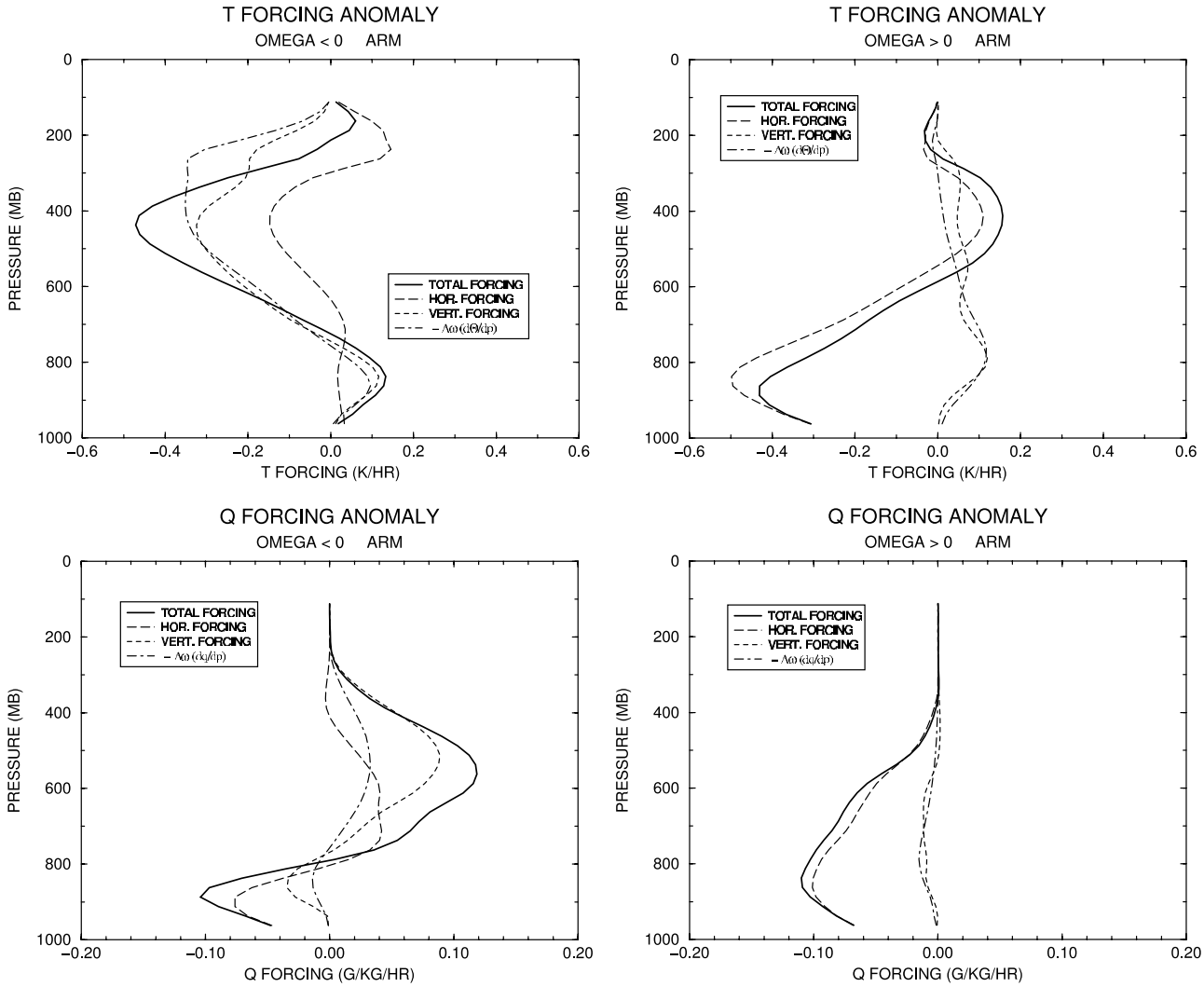

Figure 6. Contributions to the continuous forcing anomaly profiles: Total (solid), horizontal advection (dashed), vertical advection (dotted), and the vertical advection component associated with the vertical velocity anomaly (dash-dot). Upper panels show temperature advection, and lower panels show moisture advection. Left panels, $\omega < 0$; upper panels, $\omega > 0$.

only to the thermodynamic state in the column and are not informed by the specific large-scale dynamical processes that determine that instantaneous state. The standard protocol for driving SCMs in fact specifies only the total advective tendency, not its individual components, because advective cooling/warming and moistening/drying are expected to have the same effect on clouds regardless of whether they are controlled by vertical or horizontal motions or by changes in temperature/moisture gradients.

[28] Figure 8 shows composite false-color satellite images of the SGP region for most of the ISCCP cases included in the anomaly subset for upwelling situations. Red denotes visible channel, green represents the water vapor channel, and blue indicates the window thermal infrared channel. Thus white areas in the images represent high thick clouds, blue areas are cirrus, red areas are stratus/stratocumulus, and green areas tend to be clear but have high humidity. Not surprisingly, many of the relevant cases correspond to the passage of fronts or low pressure centers across the SGP site, some notable examples being 1800 9 December 1999, 1800 26 January 2000, 2100 22 February 2000, 1500 and 1800 2 March 2000, 1800 22 March 2000, and 1500 23 March 2000.

[29] Figure 9 shows similar satellite image composites for most of the ISCCP cases included in the anomaly subset for downwelling situations. Some of these examples correspond to postcold front cold air outbreaks at the SGP (1800 and 2100 11 December 2000), some occur when the wraparound region north and west of the low passes over the SGP (1800 13 February 2000, 1500 and 1800 18 February 2000), and others appear to sample the ridge crest region that precedes the approach of warm fronts (2100 26 December 1999, 1800 25 January 2000).

[30] Figures 8 and 9 reinforce the impression that the selected instances from the continuous forcing generally represent extremes of the current climate. Figure 1 shows that the climate change in advective forcing (at levels in the upper and lower troposphere for which large cloud anomalies occur) is dominated by broadening of the pdf of moisture forcing, i.e., greater occurrence of extremes, but

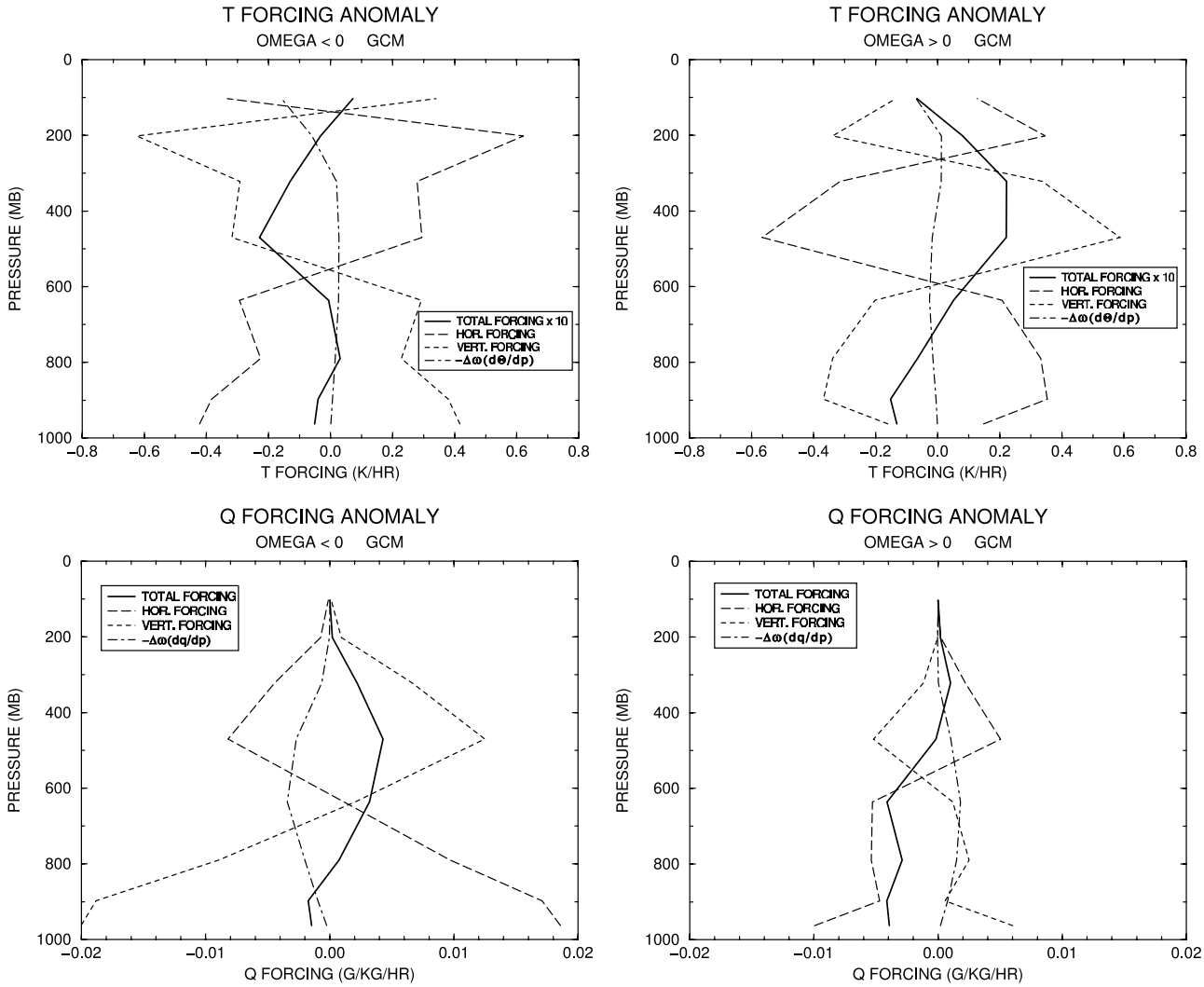

Figure 7. As in Figure 6, but for GCM climate changes in advective forcing. Note that the total T forcing anomalies are multiplied by 10 in this figure.

not so for temperature forcing, which is more a shift in the overall pdf with even a slight narrowing of the distribution.

[31] Figure 10 shows the averaged cloud anomalies that arise in response to these dynamical forcing anomalies for the $\omega < 0$ regime. ISCCP (upper left) and ARSCL (upper right) agree on the basic pattern of cloud response: high top, thick cloud amount increases, while cirrus and all low cloud types decrease. ISCCP places the cirrus and low cloud decreases at pressures ~100 mb lower than implied by the ARSCL data. The SCM (middle left and right) reproduces the general pattern of these cloud anomalies quite well; the altitudes of peak cirrus and low cloud decrease are more consistent with ARSCL than ISCCP. The SCM predicts a much larger increase in high top thick clouds than inferred from ISCCP, but not when compared to ARSCL.

[32] The bottom panels of Figure 10 show the actual cloud feedback from the GCM doubled CO_2 simulation in this regime. The GCM's cloud feedback pattern is fairly similar to the pattern of SCM anomalies, in that both predict increases in high top thick clouds and decreases in low clouds. The GCM does not predict a decrease in cirrus, consistent with the lack of cirrus in its mean state associated with its coarser vertical resolution and shallower advective forcing. The cloud increase is also at slightly higher altitude in the GCM, an expected result given that the best match moisture advection anomaly profile in the continuous forcing data set has weaker moistening in the upper troposphere than does the simulated climate change (Figure 5). Overall, though, the diagnostic technique appears to work as intended, and we might tentatively interpret the upper panels of Figure 10 as a glimpse of the actual cloud

Figure 8. False-color composite satellite image examples of the SGP region for times when advective tendency anomalies are highly correlated with GCM climate change anomalies for 500 mb $\omega < 0$. The composite images are produced by combining visible (red), water vapor channel (green), and window thermal infrared (blue) images. Time of observation is listed above each image in the format yyyymmdd.hh, where y is year, m is month, d is day, and h is hour.

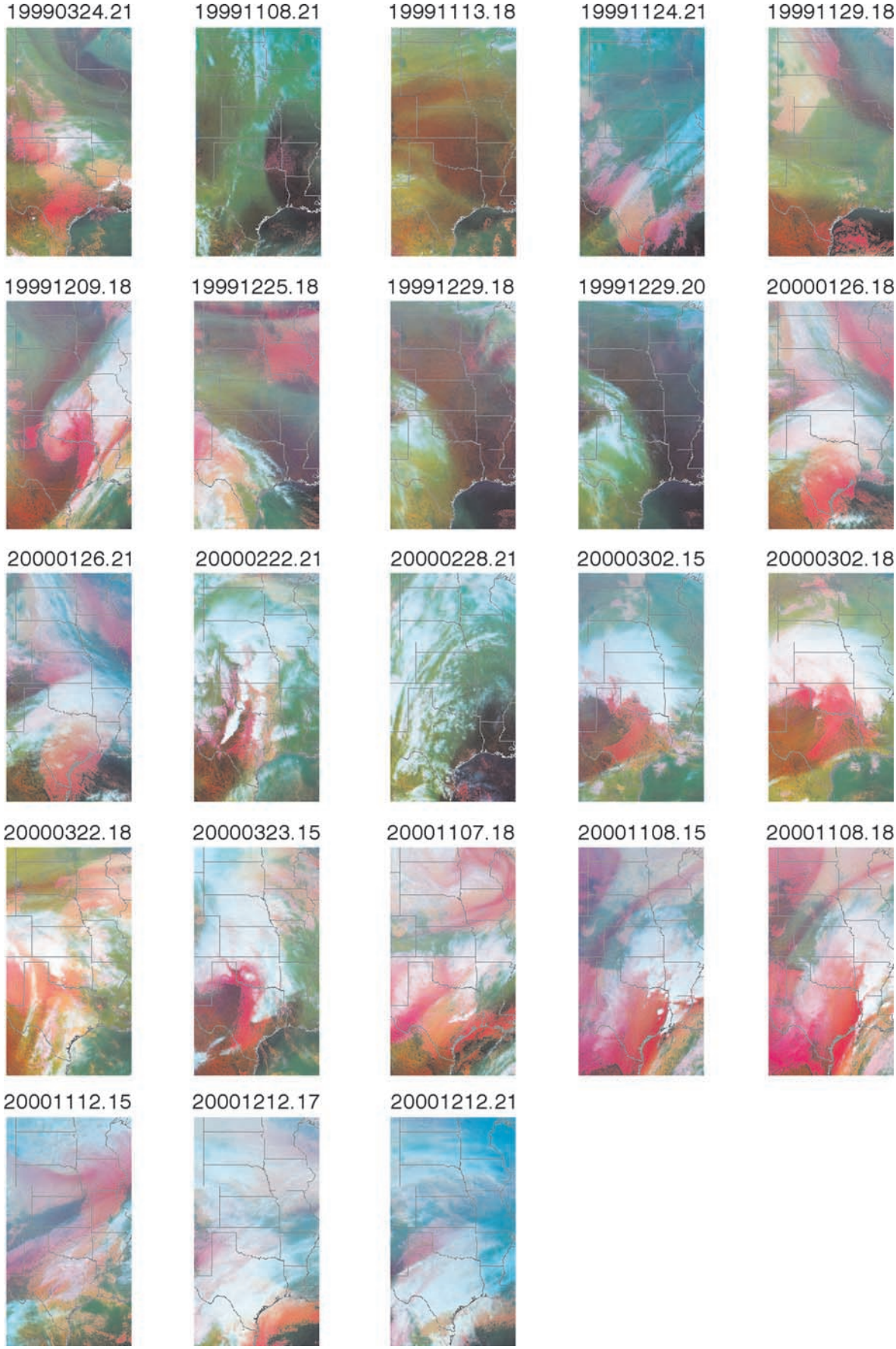
19990324.21
19991108.21
19991113.18
19991124.21
19991129.18
19991209.18
19991225.18
19991229.18
19991229.20
20000126.18
20000126.21
20000222.21
20000228.21
20000302.15
20000302.18
20000322.18
20000323.15
20001107.18
20001108.15
20001108.18
20001112.15
20001212.17
20001212.21

Figure 8

Figure 9. As in Figure 8 but for 500 mb $\omega > 0$ examples.

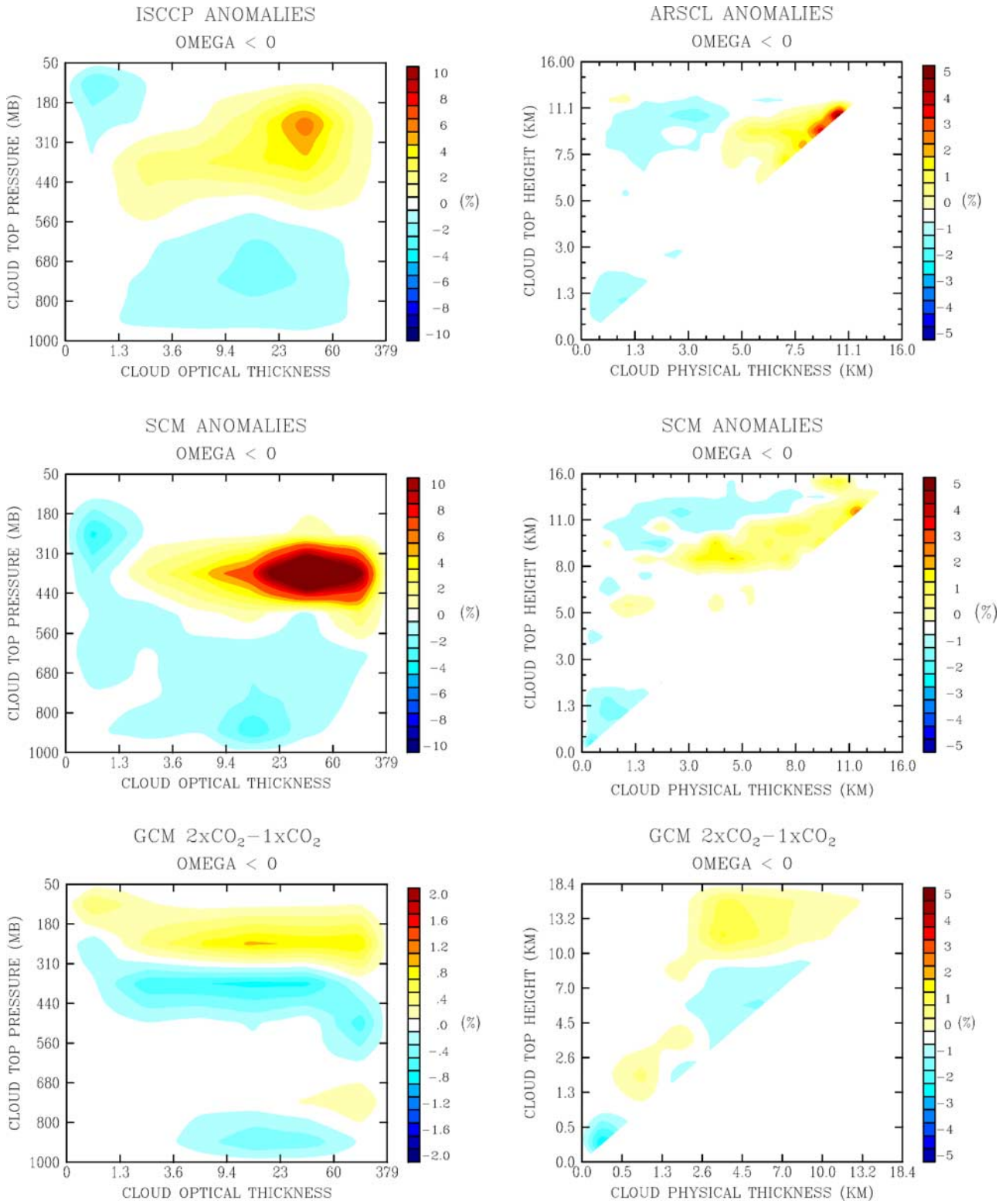

Figure 10. As in Figure 3 but for anomalies of cloud properties relative to the mean for times whose advective tendency anomalies are highly correlated with GCM climate change advection differences for 500 mb $\omega < 0$. Note the different color scale for the GCM ISCCP simulator anomalies due to the smaller climate change signal.

feedback to be expected in a warmer climate in midlatitude winter continental upwelling situations.

[33] Figure 11 shows the corresponding cloud anomalies for the $\omega > 0$ regime. The results here are less successful in terms of data set agreement, model performance and consistency between current climate variability and climate change. The ISCCP and ARSCL data (upper panels) agree that low cloud cover, mostly moderate and high optical thickness but physically thin, increases, although the same cloud top location disagreement seen in earlier figures occurs here as well. More troubling is the fundamental discrepancy in cloud type decreases. ISCCP claims that all low clouds increase while cirrus fraction decreases. ARSCL sees a weaker cirrus signal but a moderate decrease in low clouds with tops at ~2 km, i.e., it gives the impression of a downward shift and physical thinning of low clouds.

[34] The SCM (middle panels) is partly successful, given the observational uncertainty, in predicting an increase in cloudiness below ~1.5 km. However, the magnitude of this increase is less than either data set indicates and there is no sign of a downward shift in low cloud tops. In addition, the SCM produces a noisy pattern of small increases and decreases of high cloud types that is also inconsistent with the two data sets.

[35] The actual GCM cloud feedback in the warmer climate (lower panels) looks neither like the data nor the SCM. It predicts an overall decrease and an upward shift and thickening of low clouds with warming, and a slight upward shift in high clouds as well. We show later that this is due to differences in the advective forcing driving the changes. It can be seen in Figure 5 that the climate change temperature forcing in particular is quite different from the best match continuous forcing anomaly profile, even though they have similar shapes. The former has moderate upper troposphere adiabatic warming and only weak low level cooling, while the latter is dominated by strong boundary layer adiabatic cooling and only a weak upper troposphere forcing component. Thus, while the SCM versus data disagreements are useful in the sense that they highlight model inadequacies that can direct parameterization research, they cannot in general provide insight about the fidelity of the GCM's cloud feedback in these situations.

[36] Another feature worth noting is the general similarity between the GCM cloud anomalies for $\omega < 0$ and $\omega > 0$. For both regimes there is an upward shift in high clouds, a decrease in low clouds, and small changes in midlevel clouds. This is evidence that the radiative impact of doubling CO_2 affects the thermodynamic structure in all situations. The clouds, however, mostly feel this impact via the contribution of the lapse rate and humidity gradient changes to the advective anomalies, since the $2 \times CO_2$ equilibrium radiative heating anomaly itself is very small. Dynamics merely modulates the basic climate change signal, amplifying the high cloud change in upwelling environments and the low cloud change in downwelling environments. At first glance this may seem at odds with the very different advective forcing anomaly profiles for upwelling and downwelling in Figure 5. Closer inspection of these reveals that the largest forcing differences are in midtroposphere, where the GCM is too dry to have many clouds and thus responds weakly to advective forcing changes, whereas in the upper and lower troposphere the advective anomalies are more similar for upwelling and downwelling, leading to same-sign cloud changes. A different model with greater midlevel cloud amounts might exhibit greater sensitivity of its cloud feedback to the sign of the vertical velocity. However the ARSCL data, which show the direct response to the advection, also indicate little midtroposphere cloud change in response to very different advection anomalies for $\omega < 0$ and $\omega > 0$ (Figures 10 and 11). The similar midtroposphere cloud response of the SCM (Figures 10 and 11) suggests that this aspect of its behavior is realistic. The GCM's midtroposphere cloud response is a bit larger (Figures 10 and 11), but only because of its coarse vertical resolution, as we will see in the following section.

[37] The total cloud feedback is the combined result of changes in clouds in each vertical velocity regime weighted by the regime's frequency of occurrence (61% for $\omega < 0$, 39% for $\omega > 0$), plus a contribution from changes in regime occurrence frequency. In the $2 \times CO_2$ climate, $\omega < 0$ occurs 0.6% more often than in the $1 \times CO_2$ climate. By comparison, the magnitude of cloud type occurrence changes in Figures 10 and 11 is ~20–25% relative to occurrence frequencies in the control climate. Thus the "thermodynamic" component of the cloud feedback far outweighs the "dynamic" component, as also found by *Bony et al.* [2004] for the tropics, and the former is determined largely by cloud changes in large-scale upwelling environments.

5. Reconciliation of SCM-GCM Differences

[38] The similarities between the SCM and GCM cloud anomalies for $\omega < 0$ suggest that our basic premise has some validity, but differences in the details of the high cloud response, and the more fundamental low cloud anomaly disagreement for $\omega > 0$, cast doubt on the method's more general utility. What are the effects of the SCM-GCM resolution difference? Are some cloud feedbacks independent of the CO_2-driven advective forcing changes?

[39] To address the first question we degraded the SCM and continuous forcing vertical resolution to that of the GCM and repeated the 10-month simulation. Figures 12 and 13 show the resulting mean and anomaly cloud type distributions for both vertical velocity regimes. Coarse vertical resolution explains the absence of physically thin high clouds in the GCM mean state. It also accounts for part of the high cloud anomaly difference for $\omega < 0$; the coarse resolution SCM high cloud increase is centered at ~310 mb, still lower than the GCM's (180–310 mb) but higher than the 35-layer SCM (310–440 mb). The GCM's tendency to produce some midlevel mean cloudiness for $\omega > 0$ occurs too in the coarse resolution SCM. Finally, the GCM predictions for $\omega > 0$ of increasing cloud above 10 km, decreasing cloud from ~4–8 km, and increasing cloud from ~1–4 km, are all reproduced qualitatively by the coarse resolution SCM.

[40] The remaining discrepancies (sign of the cirrus change and altitude of the peak thick high cloud increase for $\omega < 0$, and sign of the change in the lowest altitude clouds for $\omega > 0$), are all consistent with deviations of the best match continuous forcing anomaly profiles from those for the climate change. The cirrus signal is easiest to understand; with a dry and cirrus-deficient GCM upper troposphere control climate, it responds to the upper level moistening

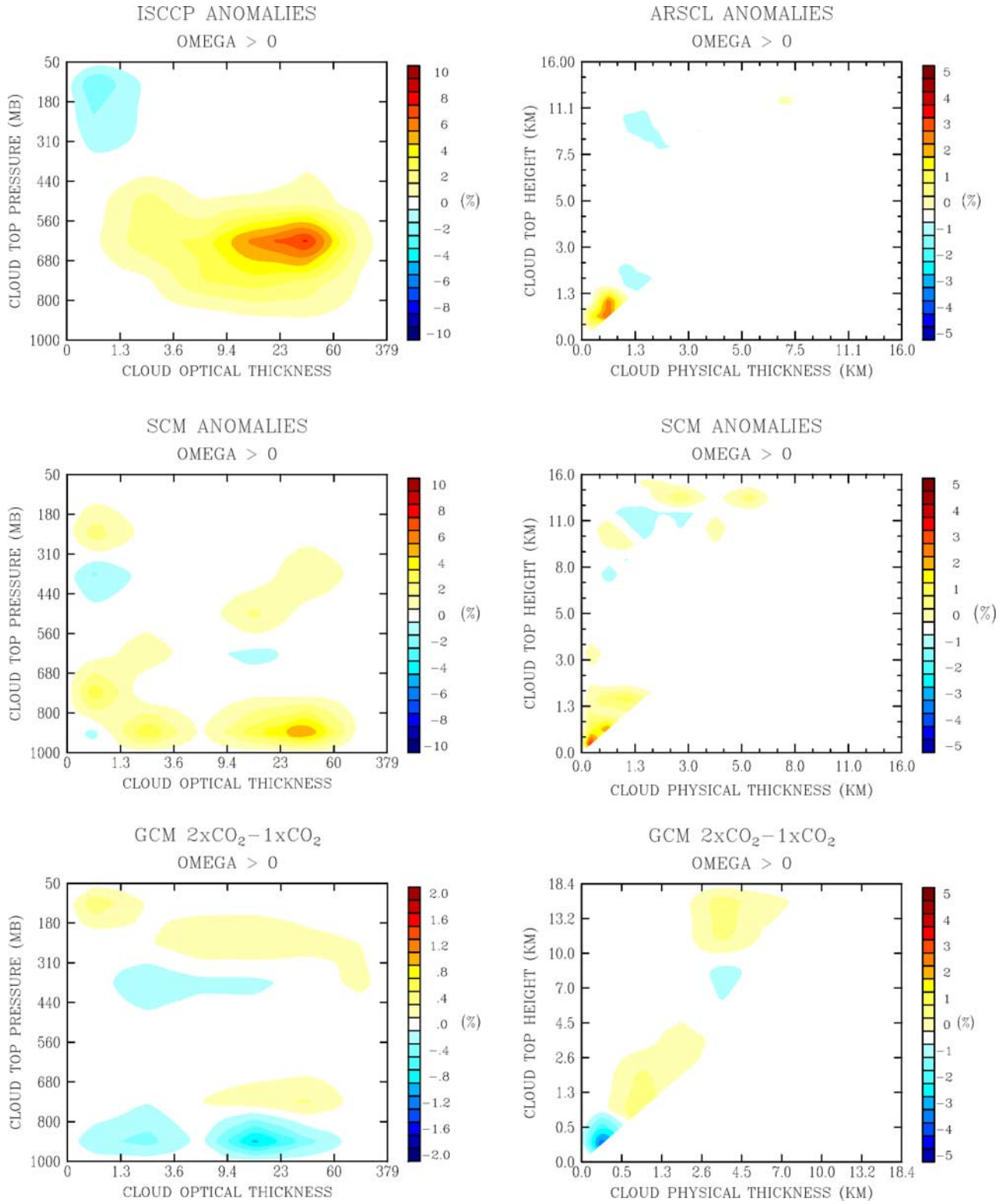

Figure 11. As in Figure 10 but for 500 mb $\omega > 0$.

of the warmer climate by making cirrus. The SCM, however, with realistic advective forcing and cirrus amount, responds to stronger forcing partly by thickening existing clouds, reducing the occurrence of the thinnest categories.

[41] To address the other two problems we searched for continuous forcing profiles that better matched the climate change advection changes only in the upper or lower troposphere, but not simultaneously. We found no better upper troposphere matches for $\omega < 0$ than those in Figure 5. In the lower troposphere we fared better. Figure 5 shows that the warmer climate has weak low-level cooling while our best continuous forcing match for $\omega > 0$ has much

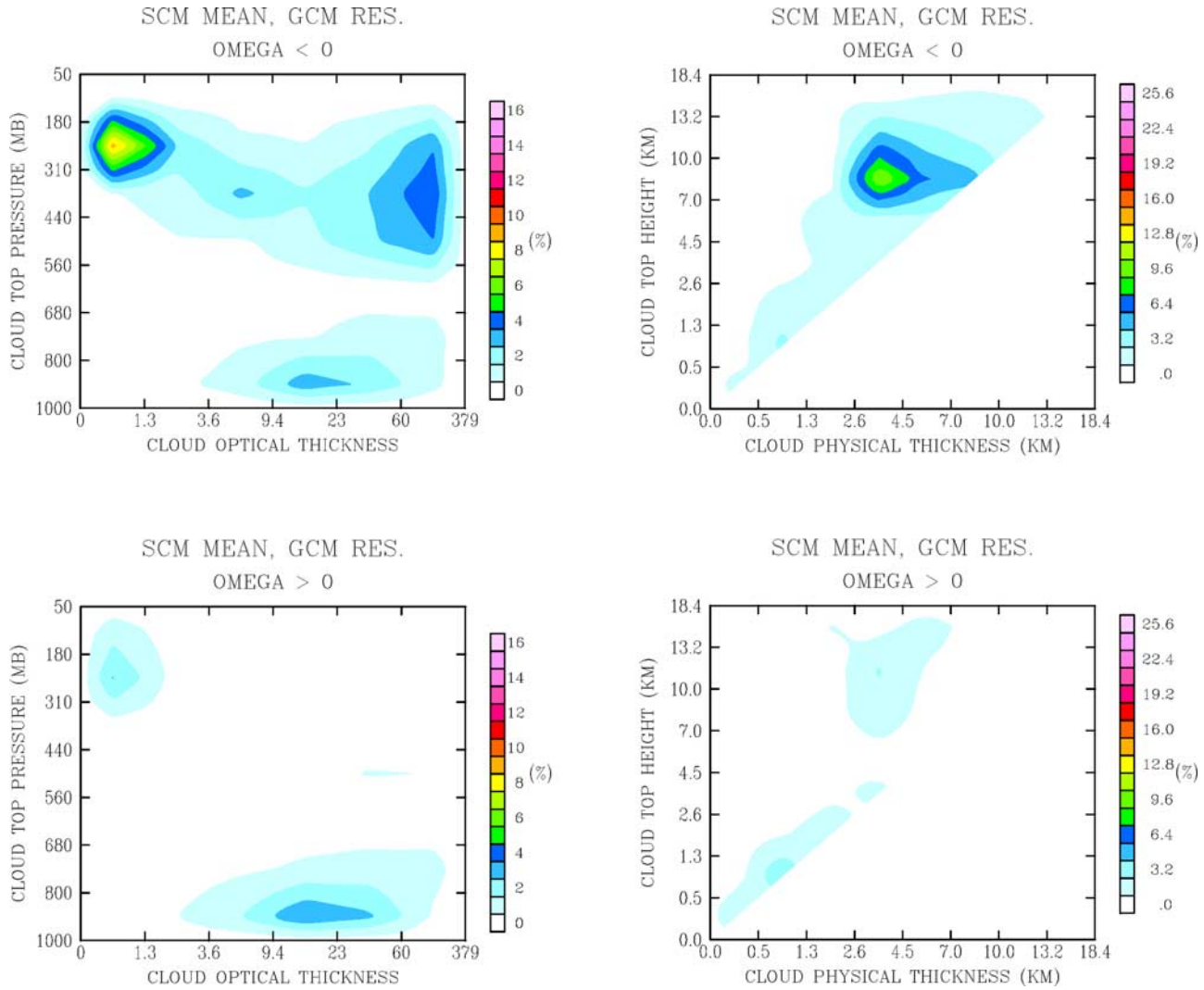

Figure 12. Mean cloud type distributions for the SCM run at the same vertical resolution as the GCM for $\omega < 0$ (upper panels) and $\omega > 0$ (lower panels). Left panels, ISCCP simulator; right panels, ARSCL simulator.

stronger low-level cooling. We were able to find continuous forcing low-level cooling anomalies more similar to those for the climate change, albeit at the expense of somewhat degraded moisture advection and upper level forcing signatures. The SCM and ARSCL cloud anomalies for these times are shown in Figure 14. The SCM now simulates a cloud decrease at the lowest levels, more consistent with the GCM. However, ARSCL indicates almost no cloud anomaly at the lowest levels.

[42] We also investigated whether the GCM's own 1 × CO_2 climate contains forcing anomalies that better resemble the 2 × CO_2 forcing changes than do the continuous forcing anomalies. We find the GCM control climate to qualitatively resemble the continuous forcing (and the cloud anomalies it implies) in this regard. Specifically, the GCM's current climate cooling and moistening anomalies for $\omega < 0$ are never as strong near 200 mb relative to those below as are those for the climate change. This apparent signature of an upward shift in tropopause height, which allows baroclinic wave transports to penetrate higher, is unique to the warmer climate. In general, though, we conclude that cloud feedback signatures in the GCM at this latitude indeed appear to be primarily responses to the advective forcing anomalies.

6. Simulator Sensitivity Tests

[43] We have explored several possible sources of the discrepancy in low cloud top altitude between the ISCCP and ARSCL data. Temporal sampling is not an issue; a subset of ARSCL data at 3-hourly, daytime only intervals corresponding to times of ISCCP results does not differ appreciably from the full ARSCL result, the main difference being somewhat less cirrus for $\omega < 0$. Spatial sampling could be examined by utitlizing the pixel-level ISCCP DX data, but the good agreement between ARSCL and ISCCP for other cloud types suggests that this is not an issue for the type of statistics aggregated in the present study. More likely, the differences are due to the ISCCP and ARSCL retrieval techniques.

[44] ISCCP's retrieval of cloud top pressure depends on its ability to correctly partition the observed thermal infrared

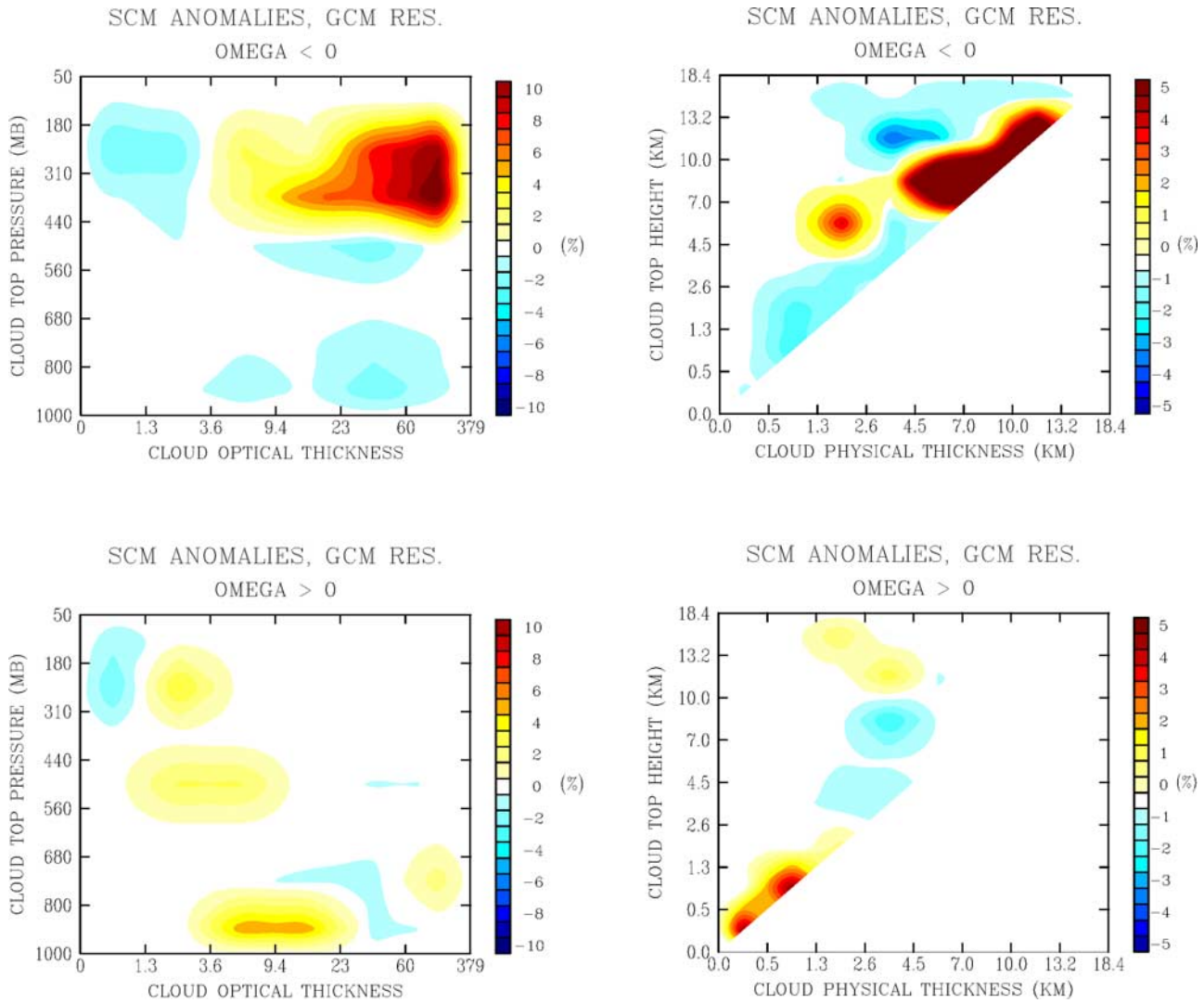

Figure 13. As in Figure 12 but for cloud type anomaly distributions.

radiance between cloudy and clear-sky contributions. This requires knowledge of the cloud optical thickness and the atmospheric temperature and humidity profiles. For very small optical thicknesses, the retrieval does not always yield a cloud top temperature consistent with the observed tropospheric temperature profile. In such cases ISCCP places the cloud in its tropopause layer. This may account for the large concentration of apparent thin cirrus clouds near the tropopause in the ISCCP results that has no obvious ARSCL counterpart.

[45] For large optical thicknesses, however, most emission is from cloud top and above. Errors in cloud top pressure in such cases may occur if the atmospheric temperature and humidity profiles are incorrect. ISCCP uses the Television Infrared Observation Satellite (TIROS) Operational Vertical Sounder (TOVS) data set for this purpose. Temperatures are provided in 15 layers from surface to stratosphere and humidity in 3 layers up to 300 mb, or are replaced by a climatology when no TOVS retrieval is available. Pressure is inferred using the hydrostatic equation. *Wang et al.* [1999] show that ISCCP cloud top pressures are biased ~60 mb low due to TOVS errors for marine stratocumulus clouds. We conducted the following tests:

[46] 1. Continuous forcing and TOVS surface pressures were compared for the cases used to produce the ISCCP anomaly composite for $\omega < 0$ in Figure 10. In most situations the TOVS surface pressure differs by ~20–30 mb from the continuous forcing, but the errors are both positive and negative and thus are unlikely to explain a systematic low bias in cloud top pressure.

[47] 2. TOVS mean temperatures at 900/620 mb are respectively 2.4/0.7 K warmer, and specific humidities 1.2/0.8 g kg^{-1} drier, than observed in the upwelling situations chosen for analysis in this paper, with instantaneous biases as large as +12 K and ±4 g kg^{-1}. We chose a case (1800 01 February 1999) in which ISCCP retrieves optically thick cloud tops primarily at 560–800 mb while ARSCL detects cloud tops primarily between 0.3–1.5 km (the 800–1000 mb layer in ISCCP). We used the ISCCP simulator to determine the effect of TOVS temperature and humidity errors. In this case TOVS temperature is biased ~5 K warm in each layer, and TOVS humidity is biased ~0.5–2 g kg^{-1} wet from ~400–850 mb and ~2 g kg^{-1} dry

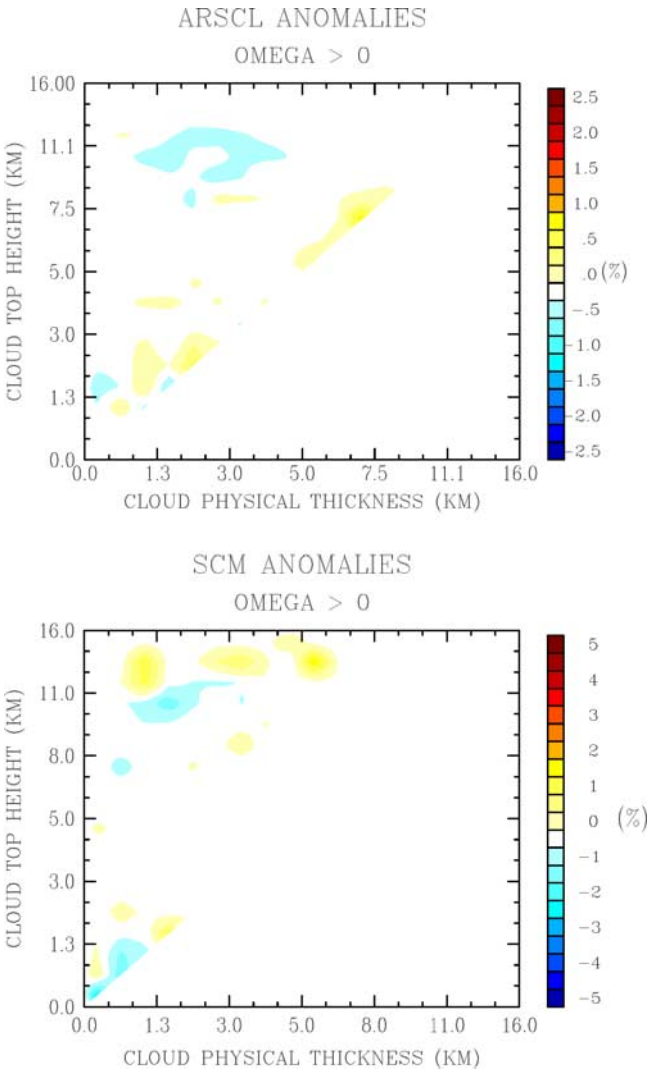

Figure 14. (top) ARSCL and (bottom) SCM cloud type distribution anomalies for $\omega > 0$ for a subset of continuous forcing times whose temperature forcing anomalies provide the best match to GCM climate change temperature forcing anomalies only below the 600 mb level.

below 850 mb. We placed a cloud of optical thickness τ = 10 into the 800–1000 mb layer with the TOVS profiles. The ISCCP simulator places the cloud in the 680–800 mb layer, qualitatively consistent with Wang et al.'s results but not enough to fully explain the discrepancy.

[48] 3. ISCCP retrievals can also be biased low by the presence of a thin high cloud above an optically thick lower cloud. For the case mentioned above, ARSCL detects no second cloud layer, but it too sometimes misses high, thin, low radar reflectivity clouds above thick low clouds. To test this hypothesis we placed a second cloud with varying optical thickness at 10 km altitude above the original low cloud. For τ = 0.5 the retrieved cloud top remains at 680–800 mb. For τ = 1 it shifts upward to the 560–680 mb layer, consistent with the actual ISCCP retrieval. For τ = 2, the diagnosed cloud top pressure is 440–560 mb. Considering that the ISCCP-ARSCL disagreement is larger in the $\omega < 0$ regime, where cirrus are more plentiful, multilayer thin cirrus-contaminated scenes combined with inaccurate TOVS atmospheric state data may explain most of the ISCCP-ARSCL difference, with both data sets missing or misidentifying some thin cirrus.

[49] We also performed ISCCP simulator sensitivity tests to understand the extent to which the unsatisfactory SCM behavior in downwelling situations (Figure 11) can be traced to differences between the actual SCM cloud field and the way it would be seen by ISCCP. First, we remapped the figure using the actual SCM cloud top pressures rather than the ISCCP radiatively adjusted ones. The ISCCP technique erroneously shifts some low clouds to high altitudes; without this the SCM indicates an overall high cloud decrease and low cloud increase. We then built on this by adding to the lowest optical thickness category the very optically thin ($\tau < 0.1$) clouds not detected at all by ISCCP. This further strengthens the impression of high (low) cloud decrease (increase). We then added nighttime clouds, which do not contribute to the ISCCP histogram results since optical thicknesses are not available. This partly offsets the effect of the first two changes. Finally, we added hourly sampling, analogous to that used for the ARSCL simulator. This has little effect except to diminish the simulated increase in tropopause cirrus. The net effect of all the changes is fairly similar to the original ISCCP simulator result.

[50] We also repeated the SCM ARSCL simulator calculations using only 1 and all 100 subgrid columns. The results are virtually indistinguishable from those in Figures 10 and 11 except for a slight bit of noise in the 1-column case. This robustness is not surprising since our ARSCL simulator results are aggregated over several hundred hours.

[51] Finally, we tested the effect of SCM overlap assumption on the ISCCP histograms. The GISS GCM radiation parameterization is equivalent to a mixed maximum-random overlap approach [*Del Genio et al.*, 1996]. In the upwelling regime (compare to Figure 10), a choice of random overlap shifts low/midlevel cloud decreases to lower optical thickness, while maximum overlap increases optically thin clouds at 680–800 mb. In the downwelling regime (compare to Figure 11), random overlap slightly intensifies the increase in low optically thick clouds, while maximum overlap causes optically thin clouds at 680–800 mb to increase while those at 310–680 mb slightly decrease. None of these changes has an overall significant effect on the SCM.

7. Discussion

7.1. Limitations and Applications

[52] The approach described in this paper assumes that the advective forcing anomalies obtained from the parent GCM are a reasonable portrayal of those that will occur in a climate change. However, this assumption is only as good as the resolved dynamics of the GCM and its simulated water vapor feedback. The GCM's mean advective forcing is too weak and shallow in upwelling regions, so a truer picture of the actual cloud feedbacks may require a higher resolution GCM with more realistic baroclinic wave structure than the one used here. In particular, coarse resolution GCMs may not be capable of simulating feedbacks in cirrus clouds (Figure 10). The water vapor feedback in the GISS

GCM is strongly positive and similar to that in other GCMs, but there is sufficient uncertainty in the magnitude of water vapor feedback to view our impressions of cloud feedback with a degree of caution. For parameterization testing purposes, though, one can choose any subset of the continuous forcing to address specific questions; it need not be limited to climate change inference.

[53] Our approach serves as a simple and useful guide to case study analysis. Case studies provide the most detailed information about processes but the cases chosen for examination may not be those from which the most can be learned. By using the SCM first to highlight areas of repeated model-data discrepancies, case studies can be chosen more judiciously to yield information that will have the most impact on the model's climate simulation. Such a strategy would be especially useful in guiding the selection of initial conditions for simulating actual weather events in GCMs as well as CRMs.

7.2. Parameterization Development Directions

[54] The comparisons between ISCCP, ARSCL, and the SCM shown in Figures 3, 4, 10, and 11 are of direct use in evaluating strengths and weaknesses of the GISS cloud parameterization in midlatitude baroclinic wave environments. We assume that ARSCL provides an overall better depiction of cloud vertical distribution and thus formation processes, while ISCCP provides the radiative property information that addresses the fidelity of SCM microphysical process representations and their link to radiation. In the following discussion we therefore discount the ISCCP tropopause thin cirrus population as a consequence of limitations in thin cloud detection and attribution, and we take ARSCL low cloud top estimates as the more accurate.

[55] In general the SCM does an excellent job of forming clouds and producing reasonable cloud amounts for different types. In 500 mb upwelling regions it successfully produces a distribution dominated by three cloud types (cirrus, high top thick clouds, and low top moderate thickness clouds) at about the right top altitudes and with a realistically broad range of simulated optical thicknesses. This is notable considering that the parameterization uses a fairly simple diagnostic scheme for predicting cloud formation and areal fraction based primarily on relative humidity and secondarily on stability [*Del Genio et al.*, 1996]. Such schemes have fallen out of favor in recent years relative to prognostic cloud cover and statistical pdf-based schemes. The two latter approaches are more physically appealing in theory but are limited in practice by an absence of observational constraints on how cloud fraction responds to changes in environmental conditions. Our results suggest that at least in midlatitude winter, diagnostic cloud cover approaches are reasonable for simulating statistical properties of cloud distributions.

[56] The SCM's main flaw in upwelling regimes is its sensitivity of high optically thick clouds to anomaly forcing (Figure 10). The same is not true of the free-standing GCM (Figure 10), suggesting that this may be associated with differences in the advective forcing. We noted earlier that the GCM's advective cooling and moistening are weaker and shallower than in the continuous forcing data set (Figure 2). This is consistent with the GCM's midlatitude winter upper troposphere dry bias and deficit of eddy kinetic energy [*Del Genio et al.*, 1996]. There are two ways this shortcoming can lead to an overestimate of high thick cloud:

[57] 1. Given the GCM's dry bias in this region, the model has difficulty making cirrus clouds. Thus the cloud scheme may err on the side of making it too difficult for cirrus to dissipate once they do form. The GISS model does not explicitly parameterize ice fallout but rather uses an autoconversion rate t^{-1} (s^{-1}) that increases with cloud water content μ, most rapidly above a specified water content μ_r = 0.1 g m^{-3} for ice clouds, as $t^{-1} = C_o\{1 - \exp[-(\mu/\mu_r)^4]\}$, with $C_o = 10^{-4}$ s^{-1} in quiescent conditions and somewhat less in the presence of large-scale upwelling. If we equate this to a rate of ice removal $t^{-1} = v_f/\Delta z$ by crystals falling at speed v_f over a model layer thickness Δz, then our parameterization implies $v_f \sim 3$ cm s^{-1} for $\mu = \mu_r$, at least an order of magnitude smaller than observed cirrus fall speeds [*Heymsfield*, 2003]. Thus, given stronger upper troposphere advective forcing like that in a warmer climate, the SCM maintains too much ice rather than allowing it to sediment out. Decreasing μ_r and increasing C_o would make the implied fall speed more realistic and might yield a better SCM simulation, but probably at the expense of making the parent GCM's simulation of its current climate worse.

[58] 2. Because of the GCM's coarse resolution, fronts are aliased to the grid scale and appear as single-grid vertical columns rather than as sloping surfaces, which gives it a tendency to have high thick clouds rather than a broader distribution of cloud types and top altitudes. Any SCM forced by synoptic-scale advective tendencies is subject to the same dilemma, since it has no input information about the ageostrophic mesoscale circulations that determine frontal cloudiness. The required increase in model resolution may not be feasible for long integrations of most current-generation climate GCMs.

[59] The SCM also underpredicts the optical thickness of cirrus clouds in upwelling regimes. The microphysics change suggested above for thick clouds would actually exacerbate this problem. It is possible that the continuous forcing advective moisture tendency is underestimated in cirrus-forming regions of the upper troposphere, given the difficulty in observing and simulating water vapor at these levels. Alternatively, the SCM's parameterization of ice crystal effective radius, which allows size to increase indefinitely solely as a function of ice water content with a fixed assumed number concentration, may be at fault. These issues may be usefully constrained when an operational version of the ARM Continuous Baseline Microphysical Retrieval product based on cloud radar and microwave radiometer information [*Miller et al.*, 2004] becomes available.

[60] In the 500 mb downwelling regime the SCM successfully reproduces the dominant low level, physically thin but moderate optical thickness, cloud type and the secondary population of cirrus (Figure 4). It has a tendency to place the low clouds slightly too low, which may contribute to its failure to simulate the downward shift in low cloudiness in response to anomaly forcing (Figure 11). This tendency is common to many GCMs. It may depend on properly linking boundary layer cloudiness and turbulence parameterizations [cf. *Lock et al.*, 2000; *Grenier and Bretherton*, 2001].

[61] The other SCM flaw in downwelling cases is its fairly random upper troposphere pattern of cloud increases and decreases in response to anomaly forcing. In most

GCMs, including the GISS model, much more attention has been paid to generating cloud in favorable, strongly forced situations than to dissipating cloud in suppressed, more weakly forced environments such as those often found behind cold fronts. The GISS scheme assumes a threshold relative humidity below which stratiform clouds cannot form. When relative humidity drops below this threshold in the presence of a preexisting cloud, the cloud water is removed instantaneously by precipitation, rather than allowing it to dissipate via evaporation over a suitable timescale. For ice clouds, cloud does not form in the GCM until the relative humidity of the potential cloud area approaches liquid water saturation (following *Sassen and Dodd* [1989]), but once formed, glaciation is assumed to reduce relative humidity to ice saturation. This may make cloud formation conditions unfavorable at the next time step if advective moistening is weak, resulting in artificial high-frequency noise in the cirrus cloud field. Recent field experiment data suggest that humidity regulation inside cirrus may often not behave in this way [*Gao et al.*, 2004].

7.3. Extension to Other Climate Regimes

[62] We chose midlatitude winter as the simplest example of cloud responses to large-scale advective forcing. However, many first-order cloud feedback issues concern deep convective and boundary-layer clouds in other climate regimes. In such regimes the advective forcing is likely to be more closely coupled to the parameterized physics, and thus GCM-derived advective tendencies will be more model-dependent and their accuracy less certain.

[63] To begin we might consider extension of the technique to summer conditions at the SGP. This potentially can give us insights into the SCM's cumulus parameterization but in a climate regime that is still significantly modulated by synoptic baroclinic wave activity that is well captured by the continuous forcing data set. A major difference between winter and summer is the importance of diurnally forced surface turbulent flux and longwave radiation effects on boundary layer temperature and moisture. One would have to add such forcing to the advective tendencies to have any reasonable hope of success.

[64] Extension of the technique to other climate regimes, e.g., marine stratocumulus and tropical maritime convection locations, must deal with the same issues as mentioned above for summer midlatitude environments. An additional difficulty is the absence of accurate advective forcing information in such locations. To use the technique in the tropics or subtropics requires using reanalysis advective tendencies as drivers for the SCM. In these regions reanalyses are relatively data-poor and influenced by the parameterizations of their own underlying GCMs. Evaluation of reanalysis time series against instantaneous satellite data, to determine for example whether tropical deep convective events and suppressed intervals are well-correlated with large-scale upwelling and downwelling, respectively, is among the highest priorities for maximizing the potential information return from the extensive cloud data sets now being accumulated by both satellites and surface remote sensing instruments.

[65] **Acknowledgments.** The authors wish to thank Shaocheng Xie, Ric Cederwall, John Yio, and Minghua Zhang for providing early access to the ARM continuous forcing product and for guidance in its use. We also thank Bill Rossow and Mark Miller for helpful discussions and Lilly del Valle for assistance in figure preparation. Three anonymous reviewers provided thoughtful reviews that helped us significantly improve the paper; section 5, for example, is a direct result of questions they raised. The satellite images in this paper were provided by Richard Wagener of the ARM External Data Center at Brookhaven National Laboratories. This research was supported by the U.S. Department of Energy Atmospheric Radiation Measurement Program and by the National Aeronautics and Space Administration Radiation Sciences Program.

References

Bony, S., J.-L. Dufresne, H. Le Treut, J.-J. Morcrette, and C. Senior (2004), On dynamic and thermodynamic components of cloud changes, *Clim. Dyn.*, *22*, 71–86.

Clothiaux, E. E., T. P. Ackerman, G. G. Mace, K. P. Moran, R. T. Marchand, M. Miller, and B. E. Martner (2000), Objective determination of cloud heights and radar reflectivities using a combination of active remote sensors at the ARM CART sites, *J. Appl. Meteorol.*, *39*, 645–665.

Del Genio, A. D., M.-S. Yao, W. Kovari, and K. K.-W. Lo (1996), A prognostic cloud water parameterization for global climate models, *J. Clim.*, *9*, 270–304.

Del Genio, A. D., W. Kovari, M.-S. Yao, and J. Jonas (2005), Cumulus microphysics and climate sensitivity, *J. Clim.*, in press.

Gao, R. S., et al. (2004), Evidence that nitric acid increases relative humidity in low-temperature cirrus clouds, *Science*, *303*, 516–520.

Grenier, H., and C. S. Bretherton (2001), A moist PBL parameterization for large-scale models and its application to subtropical cloud-topped marine boundary layers, *Mon. Weather Rev.*, *129*, 357–377.

Heymsfield, A. J. (2003), Properties of tropical and midlatitude ice cloud particle ensembles. part I: Median mass diameters and terminal velocities, *J. Atmos. Sci.*, *60*, 2573–2591.

Klein, S. A., and C. Jakob (1999), Validation and sensitivities of frontal clouds simulated by the ECMWF model, *Mon. Weather Rev.*, *127*, 2514–2531.

Lock, A. P., A. R. Brown, M. R. Bush, G. M. Martin, and R. N. B. Smith (2000), A new boundary layer mixing scheme. Part I: Scheme description and single-column model tests, *Mon. Weather Rev.*, *128*, 3187–3199.

Miller, M. A., K. L. Johnson, M. P. Jensen, G. G. Mace, X. Dong, and A. M. Vogelmann (2004), A continuous baseline microphysical retrieval (MICROBASE): Status of SGP version 1.2 and prototype TWP version, paper presented at 14th ARM Science Team Meeting, Atmos. Radiat. Measure. Prog., U.S. Dept. of Energy, Albuquerque, N. M., 22–26 March.

Rossow, W. B., and R. A. Schiffer (1999), Advances in understanding clouds from ISCCP, *Bull. Am. Meteorol. Soc.*, *80*, 2261–2288.

Sassen, K., and G. C. Dodd (1989), Haze particle nucleation simulations in cirrus clouds and application for numerical and lidar studies, *J. Atmos. Sci.*, *46*, 3005–3014.

Wang, J., W. B. Rossow, T. Uttal, and M. Rozendaal (1999), Variability of cloud vertical structure during ASTEX observed from a combination of rawinsonde, radar, ceilometer, and satellite, *Mon. Weather Rev.*, *127*, 2484–2502.

Webb, M., C. A. Senior, S. Bony, and J.-J. Morcrette (2001), Combining ERBE and ISCCP data to assess clouds in the Hadley Centre, ECMWF and LMD atmospheric climate models, *Clim. Dyn.*, *17*, 905–922.

Xie, S. C., et al. (2002), Intercomparison and evaluation of cumulus parameterizations under summertime midlatitude conditions, *Q. J. R. Meteorol. Soc.*, *128*, 1095–1135.

Xie, S., R. T. Cederwall, and M. Zhang (2004), Developing long-term single-column model/cloud system-resolving model forcing data using numerical weather prediction products constrained by surface and top of the atmosphere observations, *J. Geophys. Res.*, *109*, D01104, doi:10.1029/2003JD004045.

Yao, M.-S., and A. D. Del Genio (2002), Effects of cloud parameterization on the simulation of climate changes in the GISS GCM. Part II: Sea surface temperature and cloud feedbacks, *J. Clim.*, *15*, 2491–2503.

A. D. Del Genio, NASA Goddard Institute for Space Studies, 2880 Broadway, New York, NY 10025, USA. (adelgenio@giss.nasa.gov)

A. B. Wolf and M.-S. Yao, SGT Inc., NASA Goddard Institute for Space Studies, 2880 Broadway, New York, NY 10025, USA.